

# SelfReformer: Self-Refined Network with Transformer for Salient Object Detection

Yun Yi Ke, Lin Weisi \*

School of Computer Science and Engineering, Nanyang Technological University, Singapore  
yunyikeyk@gmail.com, wslin@ntu.edu.sg

## Abstract

The global and local contexts significantly contribute to the integrity of predictions in Salient Object Detection (SOD). Unfortunately, existing methods still struggle to generate complete predictions with fine details. There are two major problems in conventional approaches: first, for global context, high-level CNN-based encoder features cannot effectively catch long-range dependencies, resulting in incomplete predictions. Second, downsampling the ground truth to fit the size of predictions will introduce inaccuracy as the ground truth details are lost during interpolation or pooling. Thus, in this work, we developed a Transformer-based network and framed a supervised task for a branch to learn the global context information explicitly. Besides, we adopt Pixel Shuffle from Super-Resolution (SR) to reshape the predictions back to the size of ground truth instead of the reverse. Thus details in the ground truth are untouched. In addition, we developed a two-stage Context Refinement Module (CRM) to fuse global context and automatically locate and refine the local details in the predictions. The proposed network can guide and correct itself based on the global and local context generated (Fig.1), thus is named, Self-Refined Transformer (SelfReformer). Extensive experiments and evaluation results on five benchmark datasets demonstrate the outstanding performance of the network, and we achieved the state-of-the-art.

## Introduction

SOD aims to locate and segment the most attention-attractive object in a visual scene. Due to its wide applications, such as AR/VR (Qin et al. 2020) and image captioning (Xu et al. 2015; Fang et al. 2015), it has gained growing interest in recent years. Most of the state-of-the-art models are CNN-based and often have an architecture of encoder-decoder where images are firstly encoded into multi-level features, followed by a decoder for feature fusion and saliency prediction. To further improve the accuracy, most of the work tries to develop better fusion modules (Wei, Wang, and Huang 2020; Pang et al. 2020), extra refinement networks (Qin et al. 2019, 2020), utilizing different modalities like depth or contour (Zhang et al. 2020; Zhao et al. 2019), and adopting attention modules (Wang et al. 2019; Zhang et al. 2018). These methods achieved remarkable results in the SOD task. However, CNN-based networks

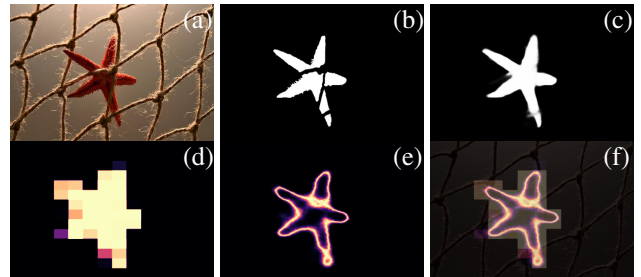


Figure 1: Visualization of global and local context obtained by our network. (a) Input, (b) Ground truth, (c) Prediction, (d) Patch-wise global context map, (e) Local context map, (f) Illustration of how global and local context benefits the prediction. Best view in color.

are limited in learning long-range relationships, resulting in a lack of global structural consistency.

In recent years, Transformer (Vaswani et al. 2017) was proposed to model long-range dependencies in language processing and was further extended to vision tasks. The vision transformers (ViT) (Yuan et al. 2021; Chu et al. 2021; Wang et al. 2021b) split the image into patches then apply multi-head self-attention and multi-layer perceptrons to capture long-range dependencies. When applied to SOD, the transformer-based networks (Liu et al. 2021; Ren et al. 2021) are effective in modeling global context, thus generating predictions with better structural integrity.

However, there are still two big challenges for better SOD. First, SOD is a densely supervised task that requires the ground truth in different resolutions for each decoder stage. Using interpolation or pooling, fine features in the ground truth are lost, and the decoder is trained against inaccurate ground truths, resulting in poor details in predictions. Noteworthy, for input size of  $224 \times 224$ , transformers like T2T-ViT (Yuan et al. 2021) and PVT (Wang et al. 2021b) usually have much smaller size of feature maps ( $56 \times 56$ ), and how to restore the fine features from this small size for accurate SOD still remain unsolved. Second, though existing studies utilizing global and local contexts like feedback network (Wei, Wang, and Huang 2020) and multi-level fusion (Pang et al. 2020), the concept of global and local context is still intuitive as we do not have a method to obtain and qualify them explicitly. Thus, finding a better representation of

\*Corresponding author.

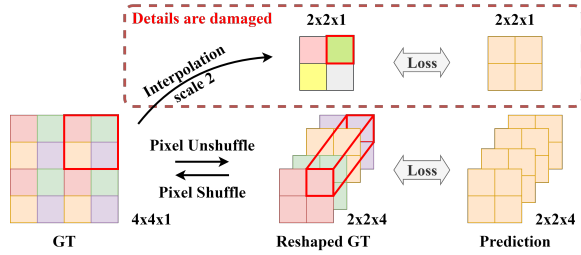


Figure 2: Illustration of conventional approach (red box) and the Pixel Shuffle (PS). Details in the GT is preserved after PS but will be lost using interpolation. Best view in color.

global and local contexts and obtaining them controllable is still an open question.

We address the abovementioned problems from three aspects. First, to preserve the structural properties of ground truth, we adopt Pixel Shuffle (PS) (Shi et al. 2016a) from Super-Resolution (SR) as the up/downsampling method. Unlike pooling or interpolation, Pixel Shuffle can reshape a high resolution (HR) image into groups of stacked low resolution (LR) images without changing the pixel values (Fig.2). Thus each decoder stage will have the same ground truth instead of multiple inconsistent LR images. Second, to obtain the global context more precisely, we reframe the SOD task into a patch-wise saliency detection problem and supervise a branch to learn the information explicitly (Fig.1d). We split input images into  $n \times n$  non-overlapping patches whereby the developed branch identifies which patch contains saliency. Compared with existing approaches where global contexts are assumed to be the high-level encoder features, in our work, the obtained global context is learned via a supervised task. Lastly, we developed a Context Refinement Module (CRM) to fuse global context features and refine local unconfident regions. The CRM will firstly fuse global contexts with decoder features for better detection completeness and generate a prediction. Then based on the unsure regions in the prediction, a local context feature map (Fig.1e) is generated to guide the network for fine structure segmentation. Thus the CRM is a two-stage module where the final predictions with a better quality were obtained based on the refinement map generated from its first predictions.

To sum up, our contributions are as follows:

- We proposed an end-to-end Transformer-based network equipped with a global and local context branch for better structural integrity and local details.
- We demonstrated that Pixel Shuffle yields better results than interpolation and pooling methods in preserving fine structures. This is the first work that applied Pixel Shuffle on the SOD task to our best knowledge.
- We introduced a method to obtain global-context information by reframing a supervised patch-wise saliency detection and developed a Context Refinement Module (CRM), which can automatically locate and refine unsure regions based on previous predictions.

## Related Work

### Global and Local Context Fusion

In encoder-decoder structure, features in deeper layers have a global view but local details are diluted because of too many convolution operations and resolution reduction, while shallower layers contain more local contexts. Many studies in SOD demonstrated that global and local context fusion can boost model performance. In SCNet (Hou et al. 2017), Hou et al. showed that global context is capable of locating the salient object while local context is for preserving details. Thus they introduced short-connection to fuse global and local information in deeper and shallower layers. Similarly, PoolNet (Liu et al. 2019) introduced a pyramid pooling module on the top of the encoder to capture the global semantic information. They further developed a feature aggregation module to recover the diluted information in the encoder and alleviate the global-context feature aggregation problem in the decoder. In PFSNet (Ma, Xia, and Li 2021), Ma et al. developed a pyramid feature shrinking module to fuse local and global features progressively. Compared with conventional encoder-decoders, where deeper stages are only fused with the next shallower stage, the pyramidal mechanism gradually fuses features across all stages, resulting in better global and local context fusion. Recently, in PA-KRN (Xu et al. 2021), Xu et al. proposed a two-stage model by firstly generating a coarse global context map to locate the salient object, followed by an attention-based sampler to zoom in the target region, and lastly refining the details by fusing local context features from encoders. It has been proved that context fusion will improve the predictions.

### Vision Transformers

Transformers were firstly introduced in natural language processing (Vaswani et al. 2017; Devlin et al. 2019; Lan et al. 2020) and were extended to vision tasks such as image classification (Dosovitskiy et al. 2021) and semantic segmentation (Zheng et al. 2021) due to their capability of modeling long-range dependencies. Networks like DETR (Carion et al. 2020) and its variants (Dai et al. 2021; Kim et al. 2021) used a combination of CNN and Transformer for various computer vision tasks (Wang et al. 2021a; Li et al. 2021). Following the Visual Transformer’s (ViT) success in image classification, which splits the input image into patches and feeds them to a transformer encoder, some studies extend the Transformer for dense prediction tasks, e.g., semantic segmentation or depth estimation. SETR (Zheng et al. 2021) and PVT (Wang et al. 2021b) employ ViT as the encoder and use several convolutional layers to upsample encoder features for dense prediction. In SOD tasks, VST (Liu et al. 2021) is the pioneer in applying visual transformers and has achieved remarkable results. In VST, T2T-ViT was adopted as the backbone where the input images were unfolded into partially overlapped patches for self-attention, and they developed a reverse T2T (rT2T) mechanism to reconstruct the predictions to the same size as the input gradually. The effectiveness of self-attention in modeling long-range dependencies makes Transformer promising in SOD tasks.

## Pixel Shuffle

Pixel Shuffle (Shi et al. 2016b) was originally applied in the task of Single Image Super-Resolution (SISR) to upscale a low-resolution (LR) image  $r$  times into a high-resolution (HR) image, and its reverse operation is Pixel-unshuffle (Fig.2). Different from interpolation methods, by reshaping the input image from  $[r^2C, H, W]$  to  $[C, rH, rW]$ , one can obtain an HR image without changing any pixel values. In SISR, the primary purpose of Pixel Shuffle is to keep the feature map at a small size to achieve a higher inference speed. Another advantage of Pixel Shuffle compared with interpolation or pooling is that we can unshuffle an HR to LR image without losing any structural details since pixels are relocated and values are unchanged. When we increase the downsampling scale using interpolation or pooling methods, more and more details are lost (Fig.3b-d); consequently, the decoder is trained against inaccurate ground truths. The shuffle and unshuffle operations ensure that details in HR ground truth remain in its LR form, regardless of scaling factors. This is useful for encoder-decoder networks as the decoder is usually densely supervised against resized ground truth. In this work, for simplicity, we use the term *Pixel Shuffle* to represent both shuffle and unshuffle operations in between layers with different scales.

## Proposed Methods

### Overall Architecture

The architecture of the network is shown in Fig.4 where we adopt PVT as the encoder backbone for better modeling of long-range dependencies. Sharing the same encoder, we developed two branches: the global-context and the local-context branches. The global-context branch is designed to obtain a rough map of the salient object. We framed a new task by predicting whether a patch of the ground truth contains saliency. In the decoder, we developed a Context Refinement Module (CRM) that fuses the features obtained in the global-context branch as a global prior knowledge for prediction and then uses its first prediction as a local refinement clue to improve fine features in the second prediction.

### Pyramid Vision Transformer (PVT) Backbone

As shown in Fig.4, input image in the shape of  $224 \times 224$  will be cut into patches for self-attention, and PVT will output four groups of features in the shape of  $56 \times 56$ ,  $28 \times 28$ ,  $14 \times 14$ , and  $7 \times 7$ . To reduce the computational complexity of the multi-head self-attention, PVT introduced a sequence reduction method to reduce the scale of  $K$  and  $V$  by firstly reshaping the input sequence  $X_i \in \mathbb{R}^{(HW \times C)}$  into  $\hat{X}_i \in \mathbb{R}^{(\frac{HW}{r} \times C \times r)}$  then apply an MLP network to reduce the channel of  $C \times r$  back to  $C$ , the process is formulated as:

$$\hat{X}_i = LN(MLP(Reshape(X, r))) \quad (1)$$

where  $LN(\cdot)$  stands for layer normalization (Ba, Kiros, and Hinton 2016). The self-attention is performed based on the reduced  $\hat{K}$  and  $\hat{V}$ :

$$Attention(Q, \hat{K}, \hat{V}) = Softmax\left(\frac{Q\hat{K}^T}{\sqrt{d_{head}}}\right)\hat{V} \quad (2)$$

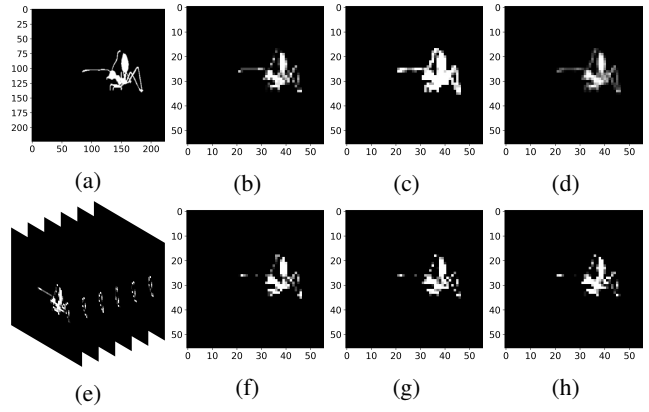


Figure 3: Visual comparisons of various downsampling methods from  $224 \times 224$  to  $56 \times 56$ . a) GT, b) bilinear interpolation, c) max pooling( $kernel = 4, stride = 4$ ), d) average pooling( $kernel = 4, stride = 4$ ), e) pixel shuffled images, f-h) examples of different channels of pixel shuffled image. Best view in zoom-in.

As a result, the total computation is reduced  $r$  times and hence more efficient.

### Obtain Better Global-Context

Global context information is crucial for the network to locate the salient object with good integrity. In encoder-decoder structure, shallower layers are responsible for reconstructing details, while deeper layers are for semantic restorations. We argue that most of the networks suffer from incomplete predictions because of two reasons: first, the ground truths are damaged (Fig.3b-d) when we use interpolation or pooling to resize them into LR for dense supervision, making it difficult for the network to learn and predict precisely. Second, some semantic information is gradually lost in the encoder due to the reduction of feature map size. Since the top-down pathway of the decoder is built upon the bottom-up encoder backbone, the high-level features will be gradually diluted in the process of being transmitted to lower layers. To tackle the first problem, we adopt Pixel Shuffle instead of interpolations or pooling methods used in existing studies. For the second issue, we employ a separate branch to specifically learn global context from input images and guide the network by fusing its features with the decoder. We explain them in detail in the following two subsections.

**Pixel Shuffle as the Up/down Sampling Method** We noticed that given the input size of  $224 \times 224$ , PVT's largest feature map size is  $56 \times 56$ , and conventional downsampling methods like interpolation or pooling are no longer viable to generate accurate ground truth images for the decoder. As shown in Fig.3, in (b), fine structures are damaged and inconsistent in the bilinear sampled ground truth. In (c) and (d), the generated GT via max and average pooling becomes inaccurate. These methods change pixel values during downsampling, resulting in inconsistent GT for each decoder stage. In contrast, Pixel Shuffle rearranges pixels into multi-channel LR images, and the structural properties

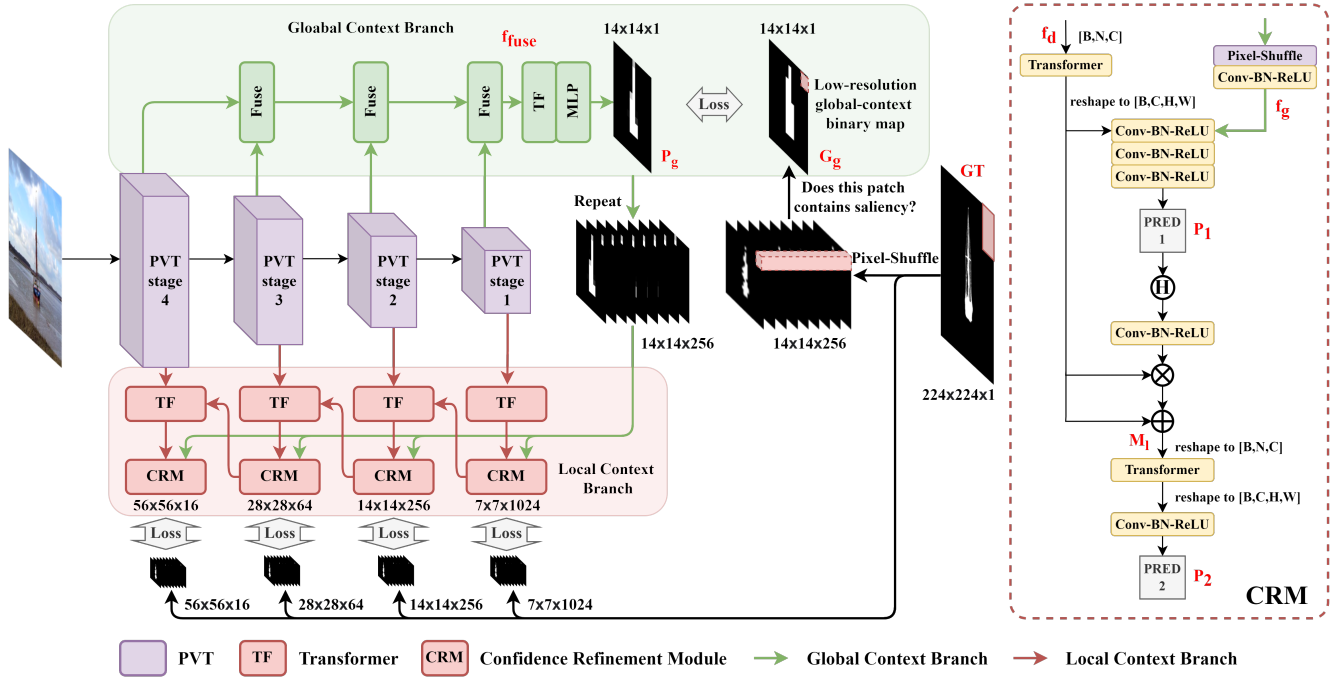


Figure 4: Network architecture for SelfReformer. Pre-trained PVT-v2 is used as the backbone. Encoder features are fed into the global context branch for patch-wise classification to obtain a low-resolution global context map. The map is further fused in CRM to locate the salient object. A CRM is developed for detail refinement where it utilizes its first prediction as a clue and generates features to improve its second prediction. In between each stage, Pixel Shuffle is applied to avoid the loss of details caused by interpolation methods.

are preserved. Though each pixel shuffled channel contains incomplete GT in (e) - (h) due to the reshaping process, the overall image is still the same once we shuffle them back to a single channel. Thus Pixel Shuffle is a more suitable method for downgrading the ground truth owing to its ability to reshape the image without changing the value. As shown in Fig.2 previously, Pixel Shuffle is to reshape an LR image into an HR image without changing any pixel values but to reduce the channels. By reversing this process, we can unshuffle an HR image into LR while preserving all the structural details. Different from all downsampling methods, by using Pixel Shuffle, we train each decoder stage against the full-scale ground truth instead of its downgraded LR images. This training scheme will enable each decoder stage to capture as much information as possible to restore the salient object. To formulate the unshuffle process, given an HR image or feature map  $I \in \mathbb{R}^{H \times W \times C}$  and a scaling factor  $r$ , it can be described as:

$$\mathcal{PS}(I_{x,y,c}, r) = I_{\lfloor x/r \rfloor, \lfloor y/r \rfloor, C \cdot r \cdot \text{mod}(y,r) + C \cdot \text{mod}(x,r) + c} \quad (3)$$

where  $x, y$  and  $c$  represent pixel coordinates and channel index in high-resolution (HR) space.

**Global-Context Branch** The global context is the clue indicating where are the salient objects. Unlike existing studies where high-level encoder features are regarded as the global context, we aim to design a supervised task to explicitly learn the information from the input image and the ground truth pair. Since in Transformer, input images are

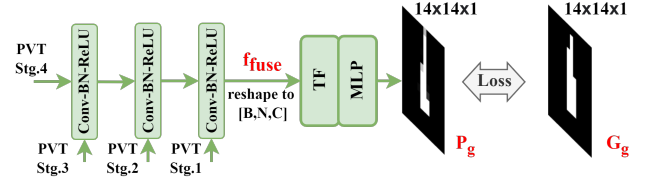


Figure 5: Global Context Branch. A patch-wise SOD task is framed to catch the global context explicitly.

split into patches, we therefore frame this supervised task as *which patch contains salient object*. The ground truth of this task can thus be easily obtained from the original ground truth images. For each patch, the branch is only required to predict a single value indicating the likelihood of the presence of the salient object, and the obtained global-context map will be passed to the decoder as guidance. Since it is a patch-wise prediction instead of full-scale pixel-wise, the designed task is easier than the salient object detection scoped for the decoder. The developed branch will contain a better representation of the global context than the decoder; thus, its features can be used as a map to guide the decoder network.

To build the branch, as shown in Fig.5, we firstly apply Pixel Shuffle to reshape all encoder features to  $14 \times 14$  then concatenate and use a few Conv-BN-ReLU layers for feature fusion. Then a transformer block  $\mathcal{TF}$  from the original Transformer and an MLP layer are employed for patch-wise

saliency prediction  $P_g$ . For simplicity, let  $f_{fuse}$  represent the fused features being passed to the Transformer, and the global context branch can be described as:

$$P_g = MLP(\mathcal{TF}(Reshape(f_{fuse}))) \quad (4)$$

where  $Reshape$  is the tensor operation from  $[B, C, H, W]$  to  $[B, H \times W, C]$ . The self-attention in  $\mathcal{TF}$  is the same as the original transformer:

$$Attention(Q, K, V) = Softmax\left(\frac{QK^T}{\sqrt{d_{head}}}\right)V \quad (5)$$

To obtain the ground truth  $G_g$  for this branch, we firstly apply Pixel Shuffle to reshape the original ground truth  $G$  from  $224 \times 224 \times 1$  to  $14 \times 14 \times 256$ , then apply  $max(\cdot)$  function along the channel dimension  $c$ :

$$G_g = \max_{c \in C}((\mathcal{PS}(G))_{i,j,c}) \quad (6)$$

where  $i, j$  and  $c$  represent pixel coordinates and channel indices. The branch is supervised using Binary Cross-Entropy(BCE) Loss:

$$\mathcal{L}_g = BCE(P_g, G_g) \quad (7)$$

The obtained map is then passed to Context Refinement Module (CRM) for fusion, and Pixel Shuffle is applied accordingly to match different scales in each decoder stage.

### Context Refinement Module (CRM)

The purpose of CRM is to fuse the global-context feature with the decoder for better semantic integrity and refine the prediction for fine details restoration. Key steps and results are shown in Fig.6 where the global context map is fused with decoder features, then a local refinement map is generated for fine feature segmentation. Thus CRM is a two-stage module where each stage generates its own predictions. To match the feature map dimension, Pixel Shuffle  $\mathcal{PS}$  is applied on the global context features  $f_g$  with different scaling factors  $r$  depending on the decoder stage. As shown in Fig.4, for the first stage of CRM, decoder features  $f_d$  are fused with  $f_g$  via a few Conv-BN-ReLU layers denoted as  $\mathcal{F}$ , and the first stage prediction  $P_1$  is then obtained and supervised against the ground truth. Mathematically, this process can be described as:

$$P_1 = \mathcal{F}(f_d, \mathcal{PS}(f_g, r)) \quad (8)$$

Similar to other SOD network predictions,  $P_1$  contains some unconfident regions in the presence of grey areas in the image. These areas are usually considered as hard pixels for the network to distinguish and usually need to employ contour or depth information for improvement. Noteworthily, due to the property of the Sigmoid function, unconfident predictions are close to 0.5 while confident predictions are close to 0 or 1. Thus by multiplying  $P_1$  with  $1 - P_1$ , the unconfident area are highlighted and the generated features can be used as a local-context map  $\mathcal{M}_l$  to guide the second stage to refine the prediction  $P_1$ . Denote the designed multiplication as  $\mathcal{H}$ , and the map is obtained as follows:

$$\mathcal{H}(P_1) = P_1 * (1 - P_1) \quad (9)$$

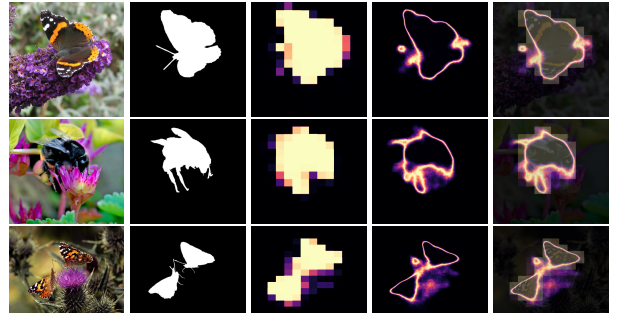


Figure 6: Illustration of fusion global and local context in CRM. From left to right: Input, Ground Truth, Global-context map, Local-context map, Overlay of global and local context. The global-context map can locate the salient object while the local-context map is to refine details.

$$\mathcal{M}_l = f_d * \mathcal{F}(\mathcal{H}(P_1)) + f_d \quad (10)$$

where  $*$  represents element-wise multiplication. We further adopt a transformer block  $\mathcal{TF}$  and a single Conv-BN-ReLU layer to generate the final prediction  $P_2$ :

$$P_2 = \mathcal{F}(\mathcal{TF}(\mathcal{M}_l)) \quad (11)$$

We apply the weighted BCE loss ( $\mathcal{L}_w$ ) for each decoder stage as used in F3Net (Wei, Wang, and Huang 2020):

$$\mathcal{L}_l = \sum_{i=1}^4 \lambda_i (\mathcal{L}_w^i(P_1, G) + \mathcal{L}_w^i(P_2, G)) \quad (12)$$

where subscript  $i$  represents each decoder stages as listed in Fig.4, and the values of  $\lambda_{1-4}$  are  $[0.5, 0.7, 0.9, 1.1]$  respectively. The total loss of the network  $\mathcal{L}$  is simply the sum of  $\mathcal{L}_g$  and  $\mathcal{L}_l$  as described above.

## Experiments

### Implementation Details

**DUTS-TR** (Wang et al. 2017) was used for training with input images resized to  $224 \times 224$ . Random horizontal flipping and  $90^\circ$  rotation were applied as the augmentation. We use pretrained PVT-v2 (Wang et al. 2021b) as the encoder. Besides, we apply Leaky ReLU (Khalid et al. 2020) for convolution layers and adopt the Adam optimizer (Kingma and Ba 2015) with default hyperparameters to train the network. Learning rates for the encoder, global context branch, and the decoder are set to  $10^{-5}$ ,  $10^{-5}$ , and  $10^{-4}$ , respectively, and they are halved every 40 epochs with a total of 200 epochs using a batch size of 16. During testing, images are resized to  $224 \times 224$ , and bilinear interpolation is applied to resize the predictions ( $224 \times 224$ ) back to the original size.

### Evaluation Datasets and Metrics

**DUT-OMRON** (Yang et al. 2013)(5168 images), **ECSSD** (Yan et al. 2013)(1000 images), **PASCAL-S** (Li et al. 2014)(850 images), **HKUIS** (Li and Yu 2015)(4447 images), and **DUTS-TE** (Wang et al. 2017)(5019 Images) are our evaluation datasets, and the evaluation metrics are as follows:

Table 1: Quantitative comparisons between our SelfReformer and other 11 methods on five benchmark datasets. Text in **bold** indicate the best performance and superscript \* stands for Transformer based network.

| Methods                          | DUTS-TE             |               |                   |                      | HKU-IS              |               |                   |                      | PASCAL-S            |               |                   |                      | ECSSD               |               |                   |                      | DUT-OMRON           |               |                   |                      |
|----------------------------------|---------------------|---------------|-------------------|----------------------|---------------------|---------------|-------------------|----------------------|---------------------|---------------|-------------------|----------------------|---------------------|---------------|-------------------|----------------------|---------------------|---------------|-------------------|----------------------|
|                                  | $F_{\beta}\uparrow$ | $M\downarrow$ | $E_{\xi}\uparrow$ | $S_{\alpha}\uparrow$ | $F_{\beta}\uparrow$ | $M\downarrow$ | $E_{\xi}\uparrow$ | $S_{\alpha}\uparrow$ | $F_{\beta}\uparrow$ | $M\downarrow$ | $E_{\xi}\uparrow$ | $S_{\alpha}\uparrow$ | $F_{\beta}\uparrow$ | $M\downarrow$ | $E_{\xi}\uparrow$ | $S_{\alpha}\uparrow$ | $F_{\beta}\uparrow$ | $M\downarrow$ | $E_{\xi}\uparrow$ | $S_{\alpha}\uparrow$ |
| F <sup>3</sup> Net <sub>20</sub> | .891                | .035          | .901              | .888                 | .936                | .028          | .952              | .917                 | .871                | .061          | .858              | .854                 | .945                | .033          | .927              | .924                 | .813                | .052          | .869              | .838                 |
| GateNet <sub>20</sub>            | .887                | .040          | .889              | .885                 | .933                | .033          | .949              | .915                 | .869                | .067          | .851              | .851                 | .945                | .040          | .924              | .919                 | .818                | .054          | .862              | .838                 |
| GCPA <sub>20</sub>               | .888                | .038          | .890              | .890                 | .938                | .030          | .949              | .920                 | .869                | .061          | .846              | .858                 | .948                | .034          | .920              | .926                 | .811                | .056          | .860              | .838                 |
| MINet <sub>20</sub>              | .883                | .037          | .897              | .884                 | .934                | .028          | .953              | .918                 | .866                | .063          | .850              | .849                 | .947                | .033          | .926              | .924                 | .809                | .055          | .864              | .832                 |
| U <sup>2</sup> Net <sub>20</sub> | .872                | .044          | .886              | .873                 | .935                | .031          | .948              | .915                 | .859                | .073          | .842              | .838                 | .951                | .033          | .924              | .927                 | .822                | .054          | .870              | .846                 |
| LDF <sub>20</sub>                | .897                | .033          | .909              | .892                 | .939                | .027          | .953              | .919                 | .874                | .059          | .865              | .856                 | .950                | .033          | .924              | .924                 | .819                | .051          | .873              | .838                 |
| MSFNet <sub>21</sub>             | .877                | .034          | .911              | .875                 | .927                | .026          | .953              | .907                 | .862                | .060          | .858              | .843                 | .941                | .033          | .926              | .914                 | .798                | .045          | .862              | .819                 |
| PFSNet <sub>21</sub>             | .896                | .036          | .902              | .892                 | .943                | .026          | .956              | .924                 | .875                | .063          | .856              | .854                 | .952                | .031          | .928              | .930                 | .823                | .055          | .875              | .842                 |
| DCN <sub>21</sub>                | .894                | .035          | .903              | .892                 | .939                | .027          | .957              | .922                 | .872                | .061          | .858              | .855                 | .952                | .031          | .929              | .928                 | .823                | .051          | .878              | .845                 |
| PAKRN <sub>21</sub>              | .906                | .032          | .916              | .900                 | .942                | .027          | .954              | .923                 | .873                | .065          | .857              | .851                 | .952                | .032          | .923              | .927                 | .834                | .049          | .885              | .853                 |
| VST <sup>*</sup> <sub>21</sub>   | .890                | .037          | .891              | .896                 | .942                | .029          | .952              | .928                 | .875                | .060          | .837              | .865                 | .950                | .032          | .917              | .932                 | .824                | .057          | .861              | .850                 |
| <b>Ours<sup>*</sup></b>          | <b>.916</b>         | <b>.026</b>   | <b>.920</b>       | <b>.911</b>          | <b>.947</b>         | <b>.024</b>   | <b>.959</b>       | <b>.930</b>          | <b>.894</b>         | <b>.050</b>   | <b>.872</b>       | <b>.874</b>          | <b>.957</b>         | <b>.027</b>   | <b>.928</b>       | <b>.935</b>          | <b>.836</b>         | <b>.041</b>   | <b>.886</b>       | <b>.856</b>          |

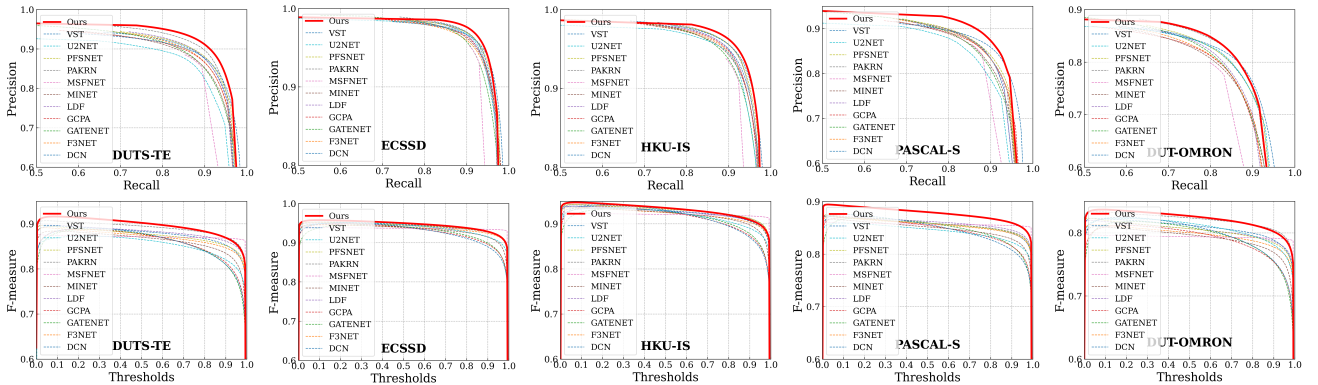


Figure 7: Precision-Recall Curves (first row) and F-measure Curves (second row) comparison on five saliency benchmark datasets. As shown above, our network achieved the best results among all networks across five datasets.

**$F_{\beta}$ -measure.** The  $F_{\beta}$ -measure (Achanta et al. 2009) is calculated by precision and recall value of saliency maps:  $F_{\beta} = \frac{(1+\beta^2) \times Precision \times Recall}{\beta^2 \times Precision + Recall}$  where  $\beta^2$  is set to 0.3 (Achanta et al. 2009).

**MAE.** MAE is the mean absolute pixel-wise differences between predictions  $x$  and ground truths  $\hat{y}$ :  $MAE = \frac{1}{n} \sum_{i=1}^n |x_i - \hat{y}_i|$ .

**E-measure.**  $E_{\xi}$  (Fan et al. 2018) calculates the similarity between the prediction and the ground truth using local pixel values and the image-wise mean.

**S-measure.**  $S_{\alpha}$  (Fan et al. 2017) aims to measure the region and object level of structural similarities between the prediction and the ground truth, denoted as  $S_o$  and  $S_r$ . It is defined as  $S_{\alpha} = \alpha S_o + (1 - \alpha) S_r$  with  $\alpha = 0.5$ .

### Comparisons with state-of-the-art

We compare our method against 11 state-of-the-art networks in the field, namely, **F<sup>3</sup>Net** (Wei, Wang, and Huang 2020), **GateNet** (Zhao et al. 2020), **GCPA** (Chen et al. 2020), **MINet** (Pang et al. 2020), **U<sup>2</sup>Net** (Qin et al. 2020), **LDF** (Wei et al. 2020), **MSFNet** (Zhang et al. 2021), **PFSNet** (Ma, Xia, and Li 2021), **DCN** (Wu, Su, and Huang 2021),

**PAKRN** (Xu et al. 2021), and **VST** (Liu et al. 2021). Results were calculated using the code provided by F<sup>3</sup>Net.

**Quantitative Evaluation.** As shown in Table.1, our network achieved the best results in all metrics calculated across the five benchmark datasets. It demonstrates outstanding performances of the proposed SelfReformer. Besides, Fig.7 shows the precision-recall curve of the above-listed networks, and our network consistently outperformed all other methods.

**Qualitative Evaluation.** Visual comparisons are listed in Fig.8. Compared with other methods, our predictions are more accurate in structural completeness and rich details (rows 1, 2, and 6). Moreover, our network excels in dealing with challenging scenarios like a small object among complex backgrounds (row 3), the unique object among its peers (row 4), and multiple salient objects (row 5).

### Ablation Studies

#### Effectiveness of global-context branch

We investigate the impact of the global-context branch by removing it and training the rest of the network. The evalu-

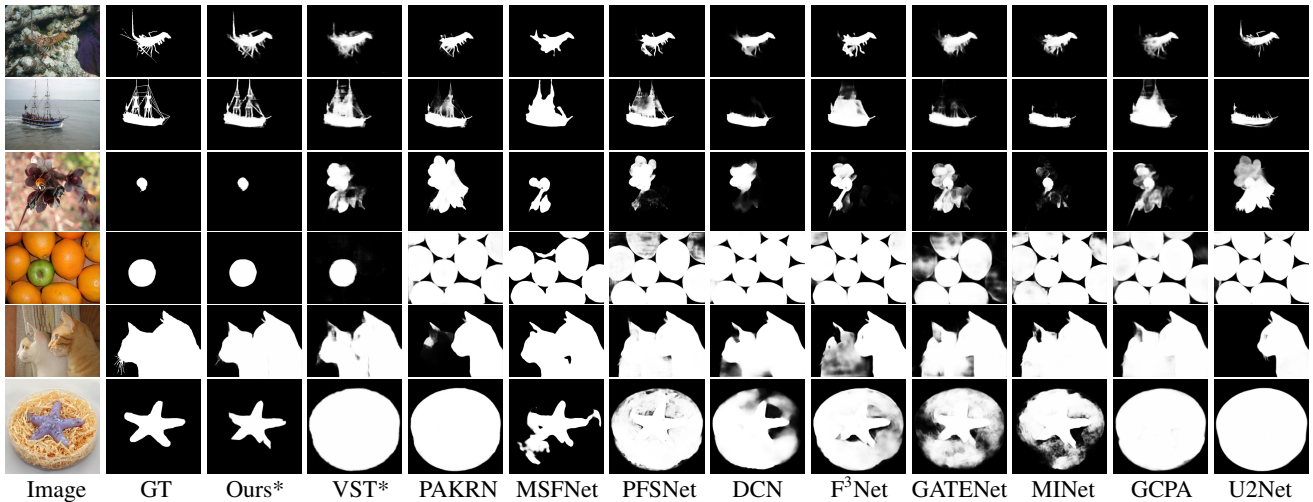


Figure 8: Visual comparisons between our method and 10 state-of-the-art networks. \* stands for Transformer based networks. More comparisons are provided in the supplementary material. Best view in zoom-in.

ation results on DUTS-TE and PASCAL-S are listed in Table 2, and we can observe significant improvement with the presence of a global context branch.

Table 2: Quantitative comparisons for the effectiveness of global-context branch.

|                    | DUTS-TE             |               |                   |                      | PASCAL-S            |               |                   |                      |
|--------------------|---------------------|---------------|-------------------|----------------------|---------------------|---------------|-------------------|----------------------|
|                    | $F_{\beta}\uparrow$ | $M\downarrow$ | $E_{\xi}\uparrow$ | $S_{\alpha}\uparrow$ | $F_{\beta}\uparrow$ | $M\downarrow$ | $E_{\xi}\uparrow$ | $S_{\alpha}\uparrow$ |
| w/o global context | .912                | .028          | .914              | .904                 | .892                | .053          | .869              | .867                 |
| w/ global context  | <b>.916</b>         | <b>.026</b>   | <b>.920</b>       | <b>.911</b>          | <b>.894</b>         | <b>.050</b>   | <b>.872</b>       | <b>.874</b>          |

### Effectiveness of CRM

Similar to the global-context branch, we compare the two predictions obtained in the CRM visually and quantitatively. Table 3 reflects the improvement in accuracy between the predictions. In Fig.9, we can observe that the second prediction is refined by the local context features generated from the first prediction. *For more ablation studies, please refer to supplementary materials.*

Table 3: Quantitative comparisons for the effectiveness of local-context branch on predictions at decoder stage 2.

| Decoder     | HKU-IS              |               |                   |                      | DUT-OMRON           |               |                   |                      |
|-------------|---------------------|---------------|-------------------|----------------------|---------------------|---------------|-------------------|----------------------|
|             | $F_{\beta}\uparrow$ | $M\downarrow$ | $E_{\xi}\uparrow$ | $S_{\alpha}\uparrow$ | $F_{\beta}\uparrow$ | $M\downarrow$ | $E_{\xi}\uparrow$ | $S_{\alpha}\uparrow$ |
| Stage 2     | .926                | .035          | .945              | .914                 | .817                | .051          | .866              | .847                 |
| First Stage | <b>.927</b>         | <b>.033</b>   | <b>.947</b>       | <b>.915</b>          | <b>.818</b>         | <b>.049</b>   | <b>.872</b>       | <b>.848</b>          |

### Conclusion

In this work, we have proposed a novel Transformer-based network named SelfReformer which can guide itself with global and local contexts. In order to obtain a better global context, we framed a supervised patch-wise saliency detection task to obtain the global feature explicitly. Meanwhile,

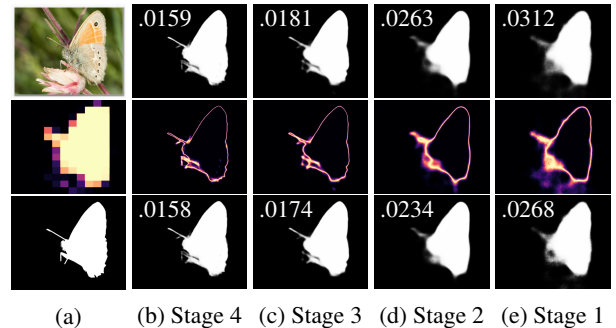


Figure 9: Qualitative comparisons for CRM. (a)top to bottom: Input, Global-context map, GT, (b)-(e)maps generated from decoder stage 4 to stage 1: first row: first stage predictions, second row: local context maps, last row: second stage predictions. MAE is marked at the top left corner. Best view in color.

since interpolation or pooling methods damage fine features in the ground truth, we adopted Pixel Shuffle as the up/downsampling method for details preservation. Besides, we developed CRM to guide the decoder with global context information and generate a local context map for better details in predictions. The proposed network demonstrated excellent performance in locating salient objects accurately with rich fine features. Evaluation results indicate the SelfReformer achieved the state-of-the-art across five benchmark datasets in all four related evaluation metrics.

### References

Achanta, R.; Hemami, S. S.; Estrada, F. J.; and Süsstrunk, S. 2009. Frequency-tuned salient region detection. In *2009 IEEE Computer Society Conference on Computer Vision and Pattern Recognition (CVPR 2009)*, 20-25 June 2009, Miami, Florida, USA, 1597–1604. IEEE Computer Society.

- Ba, L. J.; Kiros, J. R.; and Hinton, G. E. 2016. Layer Normalization. *CoRR*, abs/1607.06450.
- Carion, N.; Massa, F.; Synnaeve, G.; Usunier, N.; Kirillov, A.; and Zagoruyko, S. 2020. End-to-End Object Detection with Transformers. In Vedaldi, A.; Bischof, H.; Brox, T.; and Frahm, J., eds., *Computer Vision - ECCV 2020 - 16th European Conference, Glasgow, UK, August 23-28, 2020, Proceedings, Part I*, volume 12346 of *Lecture Notes in Computer Science*, 213–229. Springer.
- Chen, Z.; Xu, Q.; Cong, R.; and Huang, Q. 2020. Global Context-Aware Progressive Aggregation Network for Salient Object Detection. In *The Thirty-Fourth AAAI Conference on Artificial Intelligence, AAAI 2020, The Thirty-Second Innovative Applications of Artificial Intelligence Conference, IAAI 2020, The Tenth AAAI Symposium on Educational Advances in Artificial Intelligence, EAAI 2020, New York, NY, USA, February 7-12, 2020*, 10599–10606. AAAI Press.
- Chu, X.; Tian, Z.; Wang, Y.; Zhang, B.; Ren, H.; Wei, X.; Xia, H.; and Shen, C. 2021. Twins: Revisiting the Design of Spatial Attention in Vision Transformers. In Ranzato, M.; Beygelzimer, A.; Dauphin, Y.; Liang, P.; and Vaughan, J. W., eds., *Advances in Neural Information Processing Systems*, volume 34, 9355–9366. Curran Associates, Inc.
- Dai, Z.; Cai, B.; Lin, Y.; and Chen, J. 2021. UP-DETR: Unsupervised Pre-Training for Object Detection With Transformers. In *IEEE Conference on Computer Vision and Pattern Recognition, CVPR 2021, virtual, June 19-25, 2021*, 1601–1610. Computer Vision Foundation / IEEE.
- Devlin, J.; Chang, M.; Lee, K.; and Toutanova, K. 2019. BERT: Pre-training of Deep Bidirectional Transformers for Language Understanding. In Burstein, J.; Doran, C.; and Solorio, T., eds., *Proceedings of the 2019 Conference of the North American Chapter of the Association for Computational Linguistics: Human Language Technologies, NAACL-HLT 2019, Minneapolis, MN, USA, June 2-7, 2019, Volume 1 (Long and Short Papers)*, 4171–4186. Association for Computational Linguistics.
- Dosovitskiy, A.; Beyer, L.; Kolesnikov, A.; Weissenborn, D.; Zhai, X.; Unterthiner, T.; Dehghani, M.; Minderer, M.; Heigold, G.; Gelly, S.; Uszkoreit, J.; and Houlsby, N. 2021. An Image is Worth 16x16 Words: Transformers for Image Recognition at Scale. In *9th International Conference on Learning Representations, ICLR 2021, Virtual Event, Austria, May 3-7, 2021*. OpenReview.net.
- Fan, D.; Cheng, M.; Liu, Y.; Li, T.; and Borji, A. 2017. Structure-Measure: A New Way to Evaluate Foreground Maps. In *IEEE International Conference on Computer Vision, ICCV 2017, Venice, Italy, October 22-29, 2017*, 4558–4567. IEEE Computer Society.
- Fan, D.; Gong, C.; Cao, Y.; Ren, B.; Cheng, M.; and Borji, A. 2018. Enhanced-alignment Measure for Binary Foreground Map Evaluation. In Lang, J., ed., *Proceedings of the Twenty-Seventh International Joint Conference on Artificial Intelligence, IJCAI 2018, July 13-19, 2018, Stockholm, Sweden*, 698–704. ijcai.org.
- Fang, H.; Gupta, S.; Iandola, F. N.; Srivastava, R. K.; Deng, L.; Dollár, P.; Gao, J.; He, X.; Mitchell, M.; Platt, J. C.; Zitnick, C. L.; and Zweig, G. 2015. From captions to visual concepts and back. In *IEEE Conference on Computer Vision and Pattern Recognition, CVPR 2015, Boston, MA, USA, June 7-12, 2015*, 1473–1482. IEEE Computer Society.
- Hou, Q.; Cheng, M.; Hu, X.; Borji, A.; Tu, Z.; and Torr, P. H. S. 2017. Deeply Supervised Salient Object Detection with Short Connections. In *2017 IEEE Conference on Computer Vision and Pattern Recognition, CVPR 2017, Honolulu, HI, USA, July 21-26, 2017*, 5300–5309. IEEE Computer Society.
- Khalid, M.; Baber, J.; Kasi, M. K.; Bakhtyar, M.; Devi, V.; and Sheikh, N. 2020. Empirical Evaluation of Activation Functions in Deep Convolution Neural Network for Facial Expression Recognition. In *2020 43rd International Conference on Telecommunications and Signal Processing (TSP)*, 204–207.
- Kim, B.; Lee, J.; Kang, J.; Kim, E.; and Kim, H. J. 2021. HOTR: End-to-End Human-Object Interaction Detection With Transformers. In *IEEE Conference on Computer Vision and Pattern Recognition, CVPR 2021, virtual, June 19-25, 2021*, 74–83. Computer Vision Foundation / IEEE.
- Kingma, D. P.; and Ba, J. 2015. Adam: A Method for Stochastic Optimization. In Bengio, Y.; and LeCun, Y., eds., *3rd International Conference on Learning Representations, ICLR 2015, San Diego, CA, USA, May 7-9, 2015, Conference Track Proceedings*.
- Lan, Z.; Chen, M.; Goodman, S.; Gimpel, K.; Sharma, P.; and Soricut, R. 2020. ALBERT: A Lite BERT for Self-supervised Learning of Language Representations. In *8th International Conference on Learning Representations, ICLR 2020, Addis Ababa, Ethiopia, April 26-30, 2020*. OpenReview.net.
- Li, G.; and Yu, Y. 2015. Visual saliency based on multiscale deep features. In *IEEE Conference on Computer Vision and Pattern Recognition, CVPR 2015, Boston, MA, USA, June 7-12, 2015*, 5455–5463. IEEE Computer Society.
- Li, Y.; He, J.; Zhang, T.; Liu, X.; Zhang, Y.; and Wu, F. 2021. Diverse Part Discovery: Occluded Person Re-Identification With Part-Aware Transformer. In *IEEE Conference on Computer Vision and Pattern Recognition, CVPR 2021, virtual, June 19-25, 2021*, 2898–2907. Computer Vision Foundation / IEEE.
- Li, Y.; Hou, X.; Koch, C.; Rehg, J. M.; and Yuille, A. L. 2014. The Secrets of Salient Object Segmentation. In *2014 IEEE Conference on Computer Vision and Pattern Recognition, CVPR 2014, Columbus, OH, USA, June 23-28, 2014*, 280–287. IEEE Computer Society.
- Liu, J.; Hou, Q.; Cheng, M.; Feng, J.; and Jiang, J. 2019. A Simple Pooling-Based Design for Real-Time Salient Object Detection. In *IEEE Conference on Computer Vision and Pattern Recognition, CVPR 2019, Long Beach, CA, USA, June 16-20, 2019*, 3917–3926. Computer Vision Foundation / IEEE.
- Liu, N.; Zhang, N.; Wan, K.; Shao, L.; and Han, J. 2021. Visual Saliency Transformer. In *2021 IEEE/CVF International*



- Conference on Computer Vision, ICCV 2021, Montreal, QC, Canada, October 10-17, 2021, 4702–4712. IEEE.
- Ma, M.; Xia, C.; and Li, J. 2021. Pyramidal Feature Shrinking for Salient Object Detection. In *Thirty-Fifth AAAI Conference on Artificial Intelligence, AAAI 2021, Thirty-Third Conference on Innovative Applications of Artificial Intelligence, IAAI 2021, The Eleventh Symposium on Educational Advances in Artificial Intelligence, EAAI 2021, Virtual Event, February 2-9, 2021*, 2311–2318. AAAI Press.
- Pang, Y.; Zhao, X.; Zhang, L.; and Lu, H. 2020. Multi-Scale Interactive Network for Salient Object Detection. In *2020 IEEE/CVF Conference on Computer Vision and Pattern Recognition, CVPR 2020, Seattle, WA, USA, June 13-19, 2020*, 9410–9419. IEEE.
- Qin, X.; Zhang, Z. V.; Huang, C.; Dehghan, M.; Zaiane, O. R.; and Jägersand, M. 2020. U<sup>2</sup>-Net: Going deeper with nested U-structure for salient object detection. *Pattern Recognit.*, 106: 107404.
- Qin, X.; Zhang, Z. V.; Huang, C.; Gao, C.; Dehghan, M.; and Jägersand, M. 2019. BASNet: Boundary-Aware Salient Object Detection. In *IEEE Conference on Computer Vision and Pattern Recognition, CVPR 2019, Long Beach, CA, USA, June 16-20, 2019*, 7479–7489. Computer Vision Foundation / IEEE.
- Ren, S.; Wen, Q.; Zhao, N.; Han, G.; and He, S. 2021. Unifying Global-Local Representations in Salient Object Detection with Transformer. *CoRR*, abs/2108.02759.
- Shi, W.; Caballero, J.; Huszar, F.; Totz, J.; Aitken, A. P.; Bishop, R.; Rueckert, D.; and Wang, Z. 2016a. Real-Time Single Image and Video Super-Resolution Using an Efficient Sub-Pixel Convolutional Neural Network. In *2016 IEEE Conference on Computer Vision and Pattern Recognition, CVPR 2016, Las Vegas, NV, USA, June 27-30, 2016*, 1874–1883. IEEE Computer Society.
- Shi, W.; Caballero, J.; Huszar, F.; Totz, J.; Aitken, A. P.; Bishop, R.; Rueckert, D.; and Wang, Z. 2016b. Real-Time Single Image and Video Super-Resolution Using an Efficient Sub-Pixel Convolutional Neural Network. In *2016 IEEE Conference on Computer Vision and Pattern Recognition, CVPR 2016, Las Vegas, NV, USA, June 27-30, 2016*, 1874–1883. IEEE Computer Society.
- Vaswani, A.; Shazeer, N.; Parmar, N.; Uszkoreit, J.; Jones, L.; Gomez, A. N.; Kaiser, L.; and Polosukhin, I. 2017. Attention is All you Need. In Guyon, I.; von Luxburg, U.; Bengio, S.; Wallach, H. M.; Fergus, R.; Vishwanathan, S. V. N.; and Garnett, R., eds., *Advances in Neural Information Processing Systems 30: Annual Conference on Neural Information Processing Systems 2017, December 4-9, 2017, Long Beach, CA, USA*, 5998–6008.
- Wang, L.; Lu, H.; Wang, Y.; Feng, M.; Wang, D.; Yin, B.; and Ruan, X. 2017. Learning to Detect Salient Objects with Image-Level Supervision. In *2017 IEEE Conference on Computer Vision and Pattern Recognition, CVPR 2017, Honolulu, HI, USA, July 21-26, 2017*, 3796–3805. IEEE Computer Society.
- Wang, N.; Zhou, W.; Wang, J.; and Li, H. 2021a. Transformer Meets Tracker: Exploiting Temporal Context for Robust Visual Tracking. In *IEEE Conference on Computer Vision and Pattern Recognition, CVPR 2021, virtual, June 19-25, 2021*, 1571–1580. Computer Vision Foundation / IEEE.
- Wang, W.; Xie, E.; Li, X.; Fan, D.; Song, K.; Liang, D.; Lu, T.; Luo, P.; and Shao, L. 2021b. Pyramid Vision Transformer: A Versatile Backbone for Dense Prediction without Convolutions. In *2021 IEEE/CVF International Conference on Computer Vision, ICCV 2021, Montreal, QC, Canada, October 10-17, 2021*, 548–558. IEEE.
- Wang, W.; Zhao, S.; Shen, J.; Hoi, S. C. H.; and Borji, A. 2019. Salient Object Detection With Pyramid Attention and Salient Edges. In *IEEE Conference on Computer Vision and Pattern Recognition, CVPR 2019, Long Beach, CA, USA, June 16-20, 2019*, 1448–1457. Computer Vision Foundation / IEEE.
- Wei, J.; Wang, S.; and Huang, Q. 2020. F<sup>3</sup>Net: Fusion, Feedback and Focus for Salient Object Detection. In *The Thirty-Fourth AAAI Conference on Artificial Intelligence, AAAI 2020, The Thirty-Second Innovative Applications of Artificial Intelligence Conference, IAAI 2020, The Tenth AAAI Symposium on Educational Advances in Artificial Intelligence, EAAI 2020, New York, NY, USA, February 7-12, 2020*, 12321–12328. AAAI Press.
- Wei, J.; Wang, S.; Wu, Z.; Su, C.; Huang, Q.; and Tian, Q. 2020. Label Decoupling Framework for Salient Object Detection. In *2020 IEEE/CVF Conference on Computer Vision and Pattern Recognition, CVPR 2020, Seattle, WA, USA, June 13-19, 2020*, 13022–13031. Computer Vision Foundation / IEEE.
- Wu, Z.; Su, L.; and Huang, Q. 2021. Decomposition and Completion Network for Salient Object Detection. *IEEE Trans. Image Process.*, 30: 6226–6239.
- Xu, B.; Liang, H.; Liang, R.; and Chen, P. 2021. Locate Globally, Segment Locally: A Progressive Architecture With Knowledge Review Network for Salient Object Detection. In *Thirty-Fifth AAAI Conference on Artificial Intelligence, AAAI 2021, Thirty-Third Conference on Innovative Applications of Artificial Intelligence, IAAI 2021, The Eleventh Symposium on Educational Advances in Artificial Intelligence, EAAI 2021, Virtual Event, February 2-9, 2021*, 3004–3012. AAAI Press.
- Xu, K.; Ba, J.; Kiros, R.; Cho, K.; Courville, A. C.; Salakhutdinov, R.; Zemel, R. S.; and Bengio, Y. 2015. Show, Attend and Tell: Neural Image Caption Generation with Visual Attention. In Bach, F. R.; and Blei, D. M., eds., *Proceedings of the 32nd International Conference on Machine Learning, ICML 2015, Lille, France, 6-11 July 2015*, volume 37 of *JMLR Workshop and Conference Proceedings*, 2048–2057. JMLR.org.
- Yan, Q.; Xu, L.; Shi, J.; and Jia, J. 2013. Hierarchical Saliency Detection. In *2013 IEEE Conference on Computer Vision and Pattern Recognition, Portland, OR, USA, June 23-28, 2013*, 1155–1162. IEEE Computer Society.
- Yang, C.; Zhang, L.; Lu, H.; Ruan, X.; and Yang, M. 2013. Saliency Detection via Graph-Based Manifold Ranking. In *2013 IEEE Conference on Computer Vision and Pattern*

*Recognition, Portland, OR, USA, June 23-28, 2013*, 3166–3173. IEEE Computer Society.

Yuan, L.; Chen, Y.; Wang, T.; Yu, W.; Shi, Y.; Jiang, Z.; Tay, F. E. H.; Feng, J.; and Yan, S. 2021. Tokens-to-Token ViT: Training Vision Transformers from Scratch on ImageNet. In *2021 IEEE/CVF International Conference on Computer Vision, ICCV 2021, Montreal, QC, Canada, October 10-17, 2021*, 538–547. IEEE.

Zhang, M.; Liu, T.; Piao, Y.; Yao, S.; and Lu, H. 2021. Auto-MSFNet: Search Multi-scale Fusion Network for Salient Object Detection. In Shen, H. T.; Zhuang, Y.; Smith, J. R.; Yang, Y.; Cesar, P.; Metze, F.; and Prabhakaran, B., eds., *MM '21: ACM Multimedia Conference, Virtual Event, China, October 20 - 24, 2021*, 667–676. ACM.

Zhang, M.; Ren, W.; Piao, Y.; Rong, Z.; and Lu, H. 2020. Select, Supplement and Focus for RGB-D Saliency Detection. In *2020 IEEE/CVF Conference on Computer Vision and Pattern Recognition, CVPR 2020, Seattle, WA, USA, June 13-19, 2020*, 3469–3478. Computer Vision Foundation / IEEE.

Zhang, X.; Wang, T.; Qi, J.; Lu, H.; and Wang, G. 2018. Progressive Attention Guided Recurrent Network for Salient Object Detection. In *2018 IEEE Conference on Computer Vision and Pattern Recognition, CVPR 2018, Salt Lake City, UT, USA, June 18-22, 2018*, 714–722. IEEE Computer Society.

Zhao, J.; Liu, J.; Fan, D.; Cao, Y.; Yang, J.; and Cheng, M. 2019. EGNNet: Edge Guidance Network for Salient Object Detection. In *2019 IEEE/CVF International Conference on Computer Vision, ICCV 2019, Seoul, Korea (South), October 27 - November 2, 2019*, 8778–8787. IEEE.

Zhao, X.; Pang, Y.; Zhang, L.; Lu, H.; and Zhang, L. 2020. Suppress and Balance: A Simple Gated Network for Salient Object Detection. In Vedaldi, A.; Bischof, H.; Brox, T.; and Frahm, J., eds., *Computer Vision - ECCV 2020 - 16th European Conference, Glasgow, UK, August 23-28, 2020, Proceedings, Part II*, volume 12347 of *Lecture Notes in Computer Science*, 35–51. Springer.

Zheng, S.; Lu, J.; Zhao, H.; Zhu, X.; Luo, Z.; Wang, Y.; Fu, Y.; Feng, J.; Xiang, T.; Torr, P. H. S.; and Zhang, L. 2021. Rethinking Semantic Segmentation From a Sequence-to-Sequence Perspective With Transformers. In *IEEE Conference on Computer Vision and Pattern Recognition, CVPR 2021, virtual, June 19-25, 2021*, 6881–6890. Computer Vision Foundation / IEEE.